JACS
JOURNAL OF THE AMERICAN CHEMICAL SOCIETY

ARTICLE

pubs.acs.org/JACS

The Directive of the Protein: How Does Cytochrome P450 Select the Mechanism of Dopamine Formation?

Patric Schyman, Wenzhen Lai, Hui Chen, Yong Wang, and Sason Shaik*

Institute of Chemistry and the Lise Meitner-Minerva Center for Computational Quantum Chemistry, The Hebrew University of Jerusalem, 91904 Jerusalem, Israel

Supporting Information

ABSTRACT: Dopamine can be generated from tyramine via arene hydroxylation catalyzed by a cytochrome P450 enzyme (CYP2D6). Our quantum mechanical/molecular mechanical (QM/MM) results reveal the decisive impact of the protein in selecting the 'best' reaction mechanism. Instead of the traditional Meisenheimer-complex mechanism, the study reveals a mechanism involving an initial hydrogen atom transfer from the phenolic hydroxyl group of the tyramine to the iron-oxo of the compound I (Cpd I), followed by a ring−π radical rebound that eventually leads to dopamine by keto−enol rearrangement. This mechanism is not viable in the gas phase since the O−H bond activation by Cpd I is endothermic and the process does not form a stable intermediate. By contrast, the in-protein reaction has a low barrier and is exothermic. It is shown that the local electric field of the protein environment serves as a template that stabilizes the intermediate of the H-abstraction step and thereby mediates the catalysis of dopamine formation at a lower energy cost. Furthermore, it is shown that external electric fields can either catalyze or inhibit the process depending on their directionality.

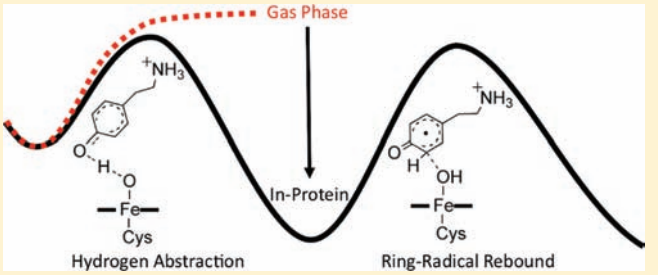

INTRODUCTION

Aromatic hydroxylation is a biologically important reaction, which is efficiently catalyzed by a variety of cytochrome P450 (CYP) enzymes.[1−4] This reaction is essential in the bioactivity of many drugs that contain aromatic rings as well as in the generation of brain neurotransmitters.[5,6] CYP2D6[5−8] is one of the most alluring of the P450 enzymes as it is involved in brain chemistry and in the metabolism of almost one-third of all drugs on the market today.[1−4] In the brain, CYP2D6 takes part in the wake−sleep cycle when serotonin is regenerated from melatonin.[9−11] It also synthesizes dopamine[12,13] (**3** in Scheme 1) directly from tyramine or in two consecutive steps from 4-methoxy-phenethylamine (**1**), which first gets demethylated to the dopamine precursor tyramine (**2**), which in turn appears to undergo aromatic hydroxylation to thereby yield dopamine.

The active P450 species, believed to be involved in most hydroxylation reactions, is the π−cation radical ferryl-oxo compound named compound I (Cpd I).[3,4,14−19] In the traditional mechanism,[1−4,20−24] shown in Scheme 2a, aromatic hydroxylation starts with the insertion of the iron-oxo of Cpd I into the aromatic ring to form the Meisenheimer-complex intermediate in the rate-limiting step. In the following step, the ipso-position proton will be transferred to the ipso-oxo atom, for example, by an initial transfer to the porphyrin nitrogen, from where it shifts to the ipso-oxo atom in the so-called proton shuttle mechanism.[20]

However, although CYP2D6 can perform many different reaction types and accepts many different substrates,[5,6] its active site has special characteristics that may inhibit certain types of reactions, such as arene hydroxylation via the mechanism described in Scheme 2a. Specifically, Glu216 and/or Asp301 that are located in the pocket over the heme[25] can hold the NH_3^+ tail of tyramine by salt bridges and may thereby contribute indirectly to inhibition of the direct oxygenation of the ortho position (see later). Moreover, the protein residues possess oriented electric fields[26,27] that may bring about new mechanisms, which are otherwise unfavorable. As shall be shown herein by means of hybrid QM/MM calculations, this is precisely the case in the ring hydroxylation of tyramine, wherein the enzyme disfavors the traditional Meisenheimer-complex mechanism but prefers the mechanism shown in Scheme 2b, whereby Cpd I abstracts the hydrogen of the hydroxyl group and continues by a ring−π radical rebound. Indeed, as will be demonstrated, this mechanism

Scheme 1. Stepwise Dopamine Formation

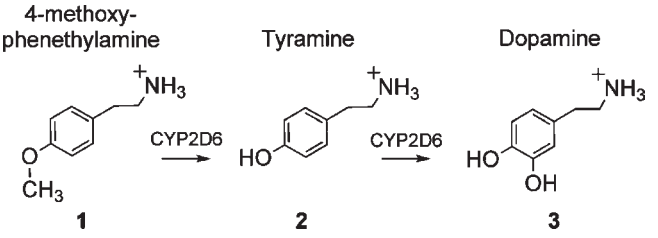

Received: February 22, 2011
Published: May 03, 2011

dx.doi.org/10.1021/ja201665x | J. Am. Chem. Soc. 2011, 133, 7977–7984

Scheme 2. Aromatic Hydroxylation Mechanisms of Tyramine by Cpd I[a]

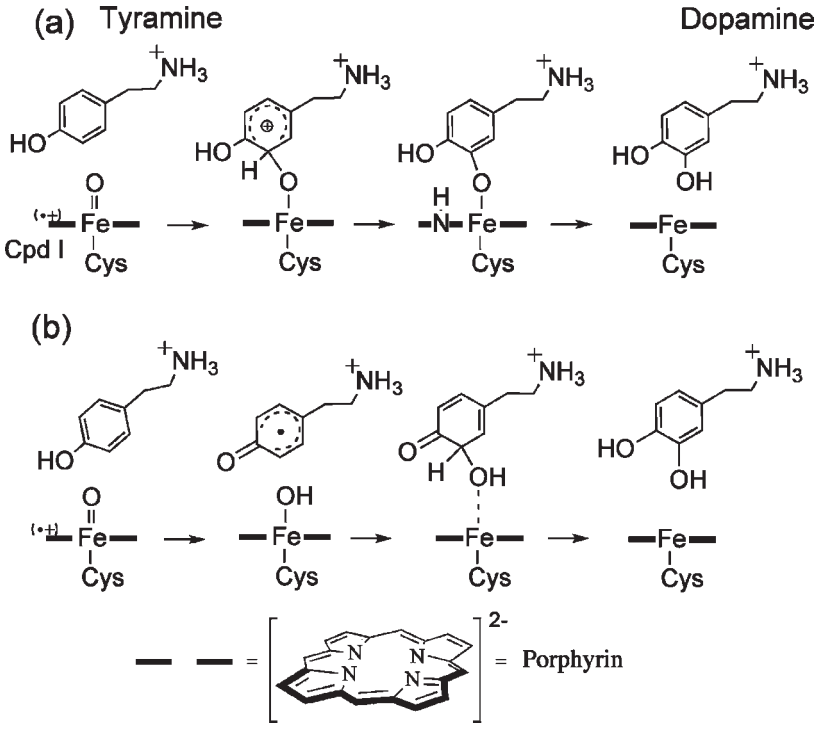

[a] While (a) represents the traditional Meisenheimer-complex mechanism, and (b) is the QM/MM-based mechanism found herein.

is impossible in the gas phase for the protonated tyramine (charged HN_3^+ tail) and is made possible only due to the local electric field of the protein that acts as a charge template for this mechanism. This is the first such demonstration for a mechanistic directive of a P450 enzyme.

METHODS

QM-Only Calculations. All our QM-only calculations are performed with density functional theory carried out with Gaussian 03.[28] Following previous studies,[29−32] Cpd I of cytochrome P450 was modeled using a porphine macrocycle without side chains and with a thiolate ligand ($(Fe^{4+}O^{2-}(C_{20}N_4H_{12})^-(SH)^-$). The spin-unrestricted UB3LYP[33−35] was employed using two basis sets: (a) LACVP(Fe)/6-31G(rest), so-called B1, to optimize the transition states and the minima without symmetry constraints, and (b) a larger basis set, TZVP[36] on all atoms, denoted B2 for single-point energy calculations. Stable species (minima) were shown to possess only positive vibrational frequencies, while transition states were ascertained to exhibit only one mode with an imaginary frequency. Bulk polarity effects mimicking the protein environment were evaluated with the polarizable continuum model (PCM) solvation model using a nonpolar solvent (chlorobenzene, ε = 5.62), and in a polar nonenzymatic environment, an aqueous medium (water, ε = 78.39) was used. The solvation cavity was created using the Pauling radii.

QM/MM Procedure. The QM/MM method has been extensively reviewed elsewhere,[37] and the QM/MM procedure used herein has been applied before;[18] therefore, only essential features are outlined below.

The tyramine substrate most likely has a protonated amino group under biological conditions.[13] The positive charge of the tyramine's amino group is essential for binding correctly in the active site of CYP2D6,[38,39] and the neutral tyramine has been observed to act as an inhibitor.[12,13] Therefore, only the protonated tyramine was considered for the QM/MM study.

During the QM/MM calculations, the QM subsystem consists of 86 atoms (see Model B in Figure 5) and involves: (i) the entire tyramine, (ii) the porphyrin without peripheral substituents and with an axial cysteine ligand, and (iii) the side chain of Asp301 residue, which forms a salt bridge with the charged amino tail of tyramine. In the water-assisted keto−enol conversion of dopamine the water molecules were added manually into the active site, thus resembling the QM-only calculations, followed by a QM/MM geometry optimization.

Setup of the Model System. Only one monomer from the X-ray structure (PDB code: 2F9Q)[25] was used, corresponding to the protein chain A in which the first eight amino acids (residues 34−41) were omitted in the calculations due to some missing segments. The removed segment of the protein is far away from the active site and has no influence on the present reaction. All other missing atoms and residues were directly added with the Swiss PDBViewer.[40] The protonation state of the amino acids was determined with the PROPKA[41] program in combination with visual inspection. The only amino acid that was altered from the normal protonation state was His376, which we judged to be protonated since it had typical hydrogen-bond distances at both nitrogen atoms. The neutral His can have a proton either at ε or δ positions of the imidazole ring, and these tautomers can only be determined by visual inspection. The following histidines were protonated at δ position (His167, His232, His324, His352, His361, His416, His419, His426, His463, and His478) and at ε position (His94, His258, and His477). After all hydrogens had been added, the structure was optimized during 2400 steps of steepest descent using the CHARMM[42] program.

The force field parameters for the heme have been described elsewhere;[18] the charges used on the ferryl-oxo moiety are Q_{Fe} = +0.63 and Q_O = −0.36. The initial topology file of the tyramine substrate was generated using Insight II 2000 (from Accelrys, San Diego), and the force field parameters were taken from the known amino acids tyrosine (phenol ring) and lysine (protonated amino tail) with a total charge of +1. The substrate was then manually modeled in a position resembling poses for other molecules, such as 5-methoxy-tryptamine, which also has a basic

dx.doi.org/10.1021/ja201665x | J. Am. Chem. Soc. 2011, 133, 7977–7984

amino group. The substrate remained in this position during the entire 3 ns of molecular dynamic (MD) simulation time (see Figure 2 and Figures S2−S4 in Supporting Information).

The Insight II software was used to add a 16 Å thick water layer. The inner 8 Å layer of water molecules was equilibrated (3 ps at 300 K) while keeping the remaining system fixed. Subsequently, more water molecules could be added, and this procedure was repeated three times until the system was saturated with water molecules. The so obtained QM/MM system consisted of 27 658 atoms. The resulting structure was then relaxed by a series of energy minimizations and MD simulations using the CHARMM force field as implemented in the CHARMM program. A 3 ns MD simulation with a time step of 1 fs was performed, during which the coordinates of the heme and the outer 8 Å layer of solvent water were kept fixed.

The QM part was treated with the unrestricted hybrid density functional UB3LYP,[33−35] and the rest of the protein and water molecules were treated with MM using the CHARMM22[43] force field through DL_POLY.[44] The basis set labeled B1 for the QM part during geometry optimization is the double-ζ LACVP basis set with a small-core ECP[45] on the iron atom and the 6-31G basis set on all other atoms (S, N, C, O, H). The energies of the B1 geometries were then refined with a larger basis set TZVP[36] on all atoms, labeled B2. The QM/MM calculations were done with the ChemShell interface software,[46] whereby the QM part was handled by Turbomole[47] and the MM part by DL_POLY.[44] The QM region interacts with the rest of the MM system by electrostatic and Lennard-Jones interactions without any cutoff. The electronic embedded scheme was used to account for the polarization effect of the QM part induced by the protein. The dangling bond at the QM—MM boundary was capped by a hydrogen link atom, and corrective terms were added by the charge-shift method.[48−50]

The QM/MM geometry optimization includes the substrate, the QM part of the Cpd I, 42 amino acid residues surrounding the substrate and heme, and 9 water molecules; for details see Table S1 in the Supporting Information. Geometry optimizations were performed with the HDLC optimizer.[51] All minima were fully optimized without symmetry restraints. The transition states were determined as the highest point on the potential energy surface along the reaction coordinates, which were scanned with a small increment of 0.02 Å near the transition states. To ascertain a continuous energy profile of the reaction, the coordinates were scanned repeatedly forward and backward until convergence for each reaction step. All the scans at the QM(B1)/MM level are collected in the Supporting Information document.

Empirical Dispersion Correction. To correct the B3LYP energies for dispersion, we used the DFT-D3 program to calculate the empirical dispersion correction (B3LYP-D).[52] As shown by Lonsdale et al,[53] dispersion correction has a large barrier lowering effect.

Deciphering the Effect of the Protein Residue on the Mechanism. To understand the final QM/MM stabilization on the mechanism in Scheme 2b, we calculated the QM system embedded in MM point charges and compared the energy with the QM/MM value. This involved a series of calculations, whereby we admitted MM residue charges in increasing radius around the QM system, until convergence. It was found that the inclusion of MM residue charges within 3 Å from the substrate converged to reproduce closely the reaction energy in the crucial step of the mechanism in Scheme 2b. Since the point charge calculation does not involve any van der Waals and/or exchange repulsion interactions, the convergence of the reaction energy to the QM/MM value is an indication that these factors make only a minor contribution. Application of PCM or conductor-like screening models (COSMO) instead of these MM residue charges did not reproduce the effect. We recall that in many previous calculations,[17,18] the use of COSMO mimicked well the bulk polarity of the protein (see Table S6 in the Supporting Information document), and as such, the failure to reproduce the effect herein indicates that we are concerned with directional electric field effect.

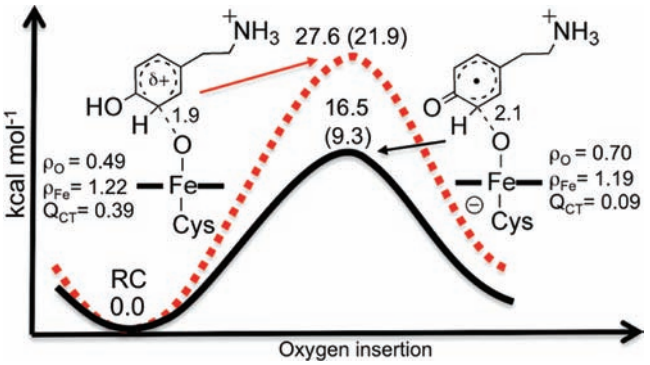

Figure 1. Oxygen insertion into tyramine (dashed red line) and into the phenoxide anion of tyramine (solid black line). Distances are in Å, and the relative energies were obtained with B3LYP/B2/MM out of parentheses and B3LYP-D/B2/MM in parentheses (D is dispersion correction). Spin densities on oxygen (O) and iron (Fe) are given at the transition state as well as the charge transferred (Q_{CT}) from the tyramine to the porphyrin.

External Electric Field (EEF). In view of the local field effect of the protein on the mechanism, we also attempted to explore the effects of an EEF on the mechanism. Following previous studies,[27a] we focused on EEFs directed along the Fe−O axis (defined as the *z* axis). These fields were created by adding point charges on two parallel circular plates on each side of the enzyme.[27a] The plates were oriented perpendicular to the Fe−O bond of Cpd I and positioned 46.8 Å from the Fe. The two plates contain 7082 point charges, each with an absolute magnitude of 0.01 e per point. These parameter settings of the charged plates (92.4 Å radius and 46.8 Å distance to Fe) produced a uniform EEF of $F_Z = \pm 0.0025$ au in the active site. This EEF is significantly smaller than the intrinsic electric field of the protein.[27b]

RESULTS

Aromatic Oxidation. Initially we studied the direct aromatic hydroxylation mechanism of tyramine in Scheme 2a. However, as shown in Figure 1, the QM/MM calculated activation energy for direct oxygen insertion is high, 27.6 kcal mol^{-1}. This barrier is ca. 7−9 kcal mol^{-1} higher than other typical aromatic hydroxylation/oxidation reactions, e.g., 18.1−21.0 kcal mol^{-1} in CYP2C9[24] or 15−18 kcal mol^{-1} in the gas phase.[20−23] Therefore, we looked for a mechanistic alternative that can account for a more facile dopamine formation. One of these alternatives was based on a recent observation that an ammonium group intensifies the acidity of the para OH group,[54] which becomes as acidic as a carboxylic group. We therefore started with a tyramine wherein the hydroxyl group was deprotonated to the phenoxide form of tyramine. The QM/MM calculations showed that the phenoxide transfers an electron to the porphyrin hole of Cpd I, and the reduced Cpd I was then inserted into the ring of the delocalized radical, see Figure 1. Although this mechanism has a low initial energy barrier, the follow-up step had a high barrier. More importantly, this mechanism was eventually ruled out since we could not identify any residue in the active site that is capable of deprotonating the hydroxyl group of tyramine.

Hydrogen abstraction (H-abstraction) from phenols is a known reaction for Cpd I species in heme and nonheme enzymes and synthetic models.[55−59] The phenolic H-abstraction is one of the main reactions of horseradish peroxidase (HRP) Cpd I with phenols.[55] Furthermore, since our group has previously shown[60]

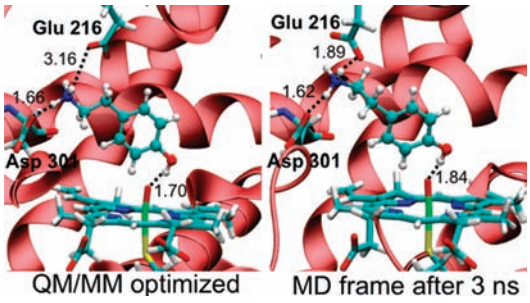

Figure 2. The substrate position including the two residues Glu216 and Asp301 in the QM/MM model (left) and after 3 ns of MD simulation (right). Note that the hydrogen bond Fe=O···HO−tyramine is retained. The used force field charges for the ferryl-oxo are Q_{Fe} = +0.63 and Q_O = −0.36.

that ethanol dehydrogenation by CYP2E1 may well be initialized by such a step, we decided to explore this mechanism for the reaction of CYP2D6 with tyramine, as schematically shown above in Scheme 2b. Indeed, our MD simulations showed that the hydrogen bond between the oxo ligand of the Cpd I and the hydroxyl group of the tyramine is sustained during the 3 ns simulation time (see Figure S2 in Supporting Information). The substrate position is also retained during the simulation with the positively charged ammonium group positioned clamped between the Glu216 and Asp301, as shown in Figure 2 (see Figures S3 and S4 in Supporting Information).

Starting from the conformation in Figure 2, we calculated the phenolic H-abstraction reaction, and the profile is shown in Figure 3. Clearly, Cpd I is indeed a potent hydrogen-atom abstractor toward the phenolic O−H. The H-abstraction barrier in Figure 3 from reactant (RC) is only 10.4 (9.7) kcal mol^{-1} (ZPE corrections are not included and would lower the energy barrier even more, by approximately 3−4 kcal mol^{-1}), and the intermediate (**IM1**) formed is relatively stable, with exothermicity of −10.8 (−9.7) kcal mol^{-1}.

The follow-up step in Figure 3 is the rebound of the phenoxy radical onto the iron−hydroxo complex, compound II (Cpd II), via the ortho position of the ring, to form the keto tautomer of dopamine. As can be seen in Figure 3, the barrier for the π−rebound step is 19.0 (14.0) kcal mol^{-1}, which is ca. 9 kcal mol^{-1} lower than the barrier for the traditional Meisenheimer-complex formation mechanism in Figure 1. In addition the rebound barrier from the **IM1** is smaller than the reverse hydrogen-transfer barrier, which will prevent unwanted backward reaction.

Water Assisted Keto−Enol Conversion of Dopamine. The keto−dopamine intermediate formed after rebound (Figure 3) is stable, and the shuttle mechanism,[20,22] transferring a proton to the porphyrin, has a very large barrier (more than 30 kcal mol^{-1}, see Table S4 in the Supporting Information) and is therefore ruled out. Directly transferring the proton from the meta position to the ketonic para oxygen is energetically very unfavorable as can be seen from Figure 4a (barrier >50 kcal mol^{-1}). Our group has noted previously[11,61] that water molecules can facilitate these 'forbidden' proton shift reactions. The question is whether this water-assisted mechanism occurs in the enzymatic pocket or on the surface where water molecules are abundant.

In fact, as shown in Figure 4b, the substrate is not actually bonded to the heme (the distance between Fe and O is 3 Å), and as such, the keto substrate may exit the pocket and be converted

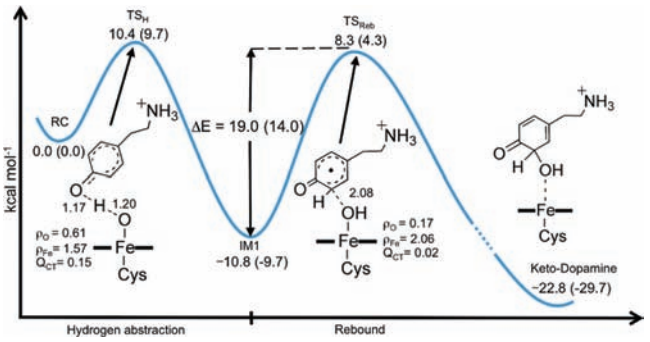

Figure 3. The H-abstraction/rebound mechanism of tyramine conversion to dopamine. Key properties of the transition states are noted: selected bond distances (Å), spin densities (ρ) on oxygen (O) and iron (Fe), and the charge transferred (Q_{CT}) from the tyramine to the porphyrin. Energies out of parentheses correspond to B3LYP/B2/MM values, while those in parentheses include dispersion (D) correction (B3LYP-D/B2/MM).

to dopamine on the surface. However, to avoid any bias, we investigated herein a water-assisted keto−enol transformation for both enzymatic and nonenzymatic reactions.

The nonenzymatic reactions were investigated using gas phase B1-optimized geometries and B2//B1 energy correction as well as solvation correction with water as a solvent. The in-protein reaction was studied with QM/MM. Figure 4a shows the different energies for one or two water-assisted proton transfers. In both environments, two water molecules are needed to make the keto−enol transformation feasible. The transition structures for the two water molecules assisted proton transfer in the gas phase and in the enzyme are similar (see Figure 4b).

One question remains regarding the in-protein process: While two water molecules do fit in the active site of our QM/MM model, can these water molecules enter the active site? Previous docking and MD studies[62] showed that during oxidation water molecules could easily move into the active site. However, during a 1 ns MD on the structure with two water molecules (see Figure 4b), the two water molecules left the active site. Therefore our results tentatively disfavor an enzymatic process and suggest that the keto−enol transformation most likely occurs on the protein surface where water is more abundant.

■ DISCUSSION

Our study reveals that aromatic hydroxylation via the usual Meisenheimer-complex mechanism is inhibited, and the protein prefers a mechanism via an initial H-abstraction from an adjacent hydroxyl group followed by a π-rebound mechanism to form the keto−enol intermediate. The activation energy for phenolic−H-abstraction by Cpd I is low, and the rate limiting step is the π-rebound with a barrier of 19.0 (14.0 with dispersion correction) kcal mol^{-1}. The key role of the phenol hydroxyl group vis-à-vis the high barrier of the Meisenheimer-complex mechanism may account for the findings[12,13] that the O-methylated substrate, 4-methoxy-phenethylamine, undergoes initial O-demethylation prior to aromatic hydroxylation (see Scheme 1). Therefore, it is important to understand the manners whereby the protein inhibits one reaction mechanism and promotes the other.

How Does the Protein Inhibit the Meisenheimer-Complex Mechanism? The high QM/MM barrier for the Meisenheimer-complex mechanism in Figure 1 is gauged relative to the reactant

dx.doi.org/10.1021/ja201665x |J. Am. Chem. Soc. 2011, 133, 7977–7984

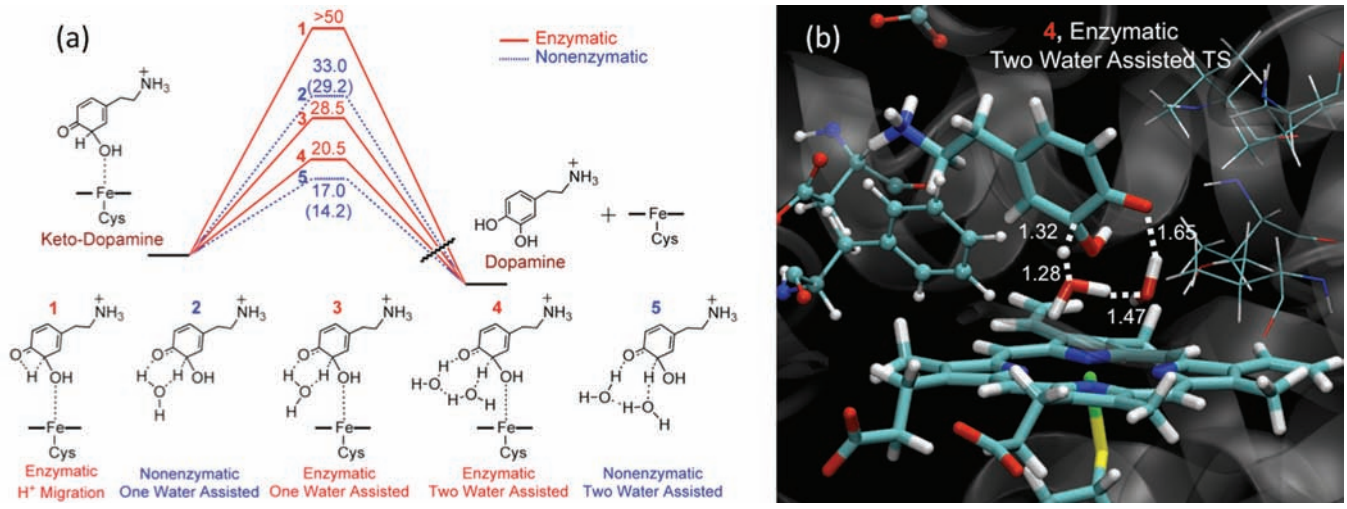

Figure 4. (a) A schematic representation of the keto→enol rearrangement process under different conditions, with numbers 1−5 referring to the respective transition states. The graph shows the influence of water molecules on the nonenzymatic and the enzymatic rearrangement barriers (kcal mol^{-1}). The enzymatic environment is calculated using QM/MM, and for the nonenzymatic environment, a continuum model (PCM) of water is used. In the enzymatic process the organic molecule is coordinated to the ferric iron of the heme. All energies were obtained with the B2 basis set, and values in parentheses include ZPE corrections. (b) The transition state for the enzymatic process, which involves two water molecules.

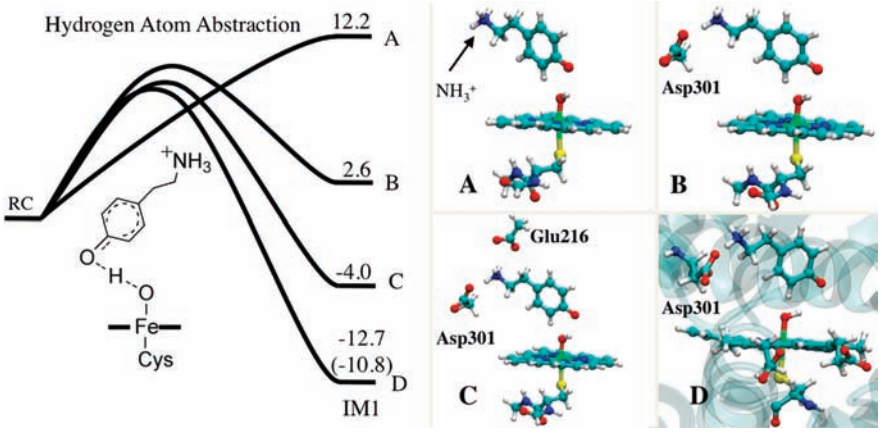

Figure 5. Relative stabilities (B2 data in kcal mol^{-1}) of the H-abstraction intermediate (**IM1**) in different environments: (A) QM-only with charged tyramine, (B) QM-only including Asp301, (C) QM-only including Asp301 and Glu216, (D) QM/MM calculation of the whole protein. Values outside of the parentheses refer to the relative QM energy including polarization from MM point charges, and values within the parentheses refer to the relative QM/MM energy.

cluster (RC). We verified that the corresponding gas-phase barrier is also large (29.8 kcal mol^{-1}) due to a very large stabilization (16.5 kcal mol^{-1}) of the corresponding RC between the protonated tyramine and Cpd I. Repeating the gas-phase calculations with the tyramine having a deprotonated tail ($CH_2CH_2NH_2$) showed a "normal" aromatic hydroxylation barrier (20.9 kcal mol^{-1}) and verified that the large barrier of the protonated tyramine is mostly due to the RC stabilization because of electrostatic interactions between the protonated tyramine and the heme. We note that the unprotonated form of tyramine functions as an inhibitor for CYP2D6,[12,13] presumably by forming the corresponding Fe−NH_2 complex, whereas the protonated tail of tyramine is required for substrate binding within the protein. Thus, the tyramine binding mechanism (via Glu216 and Asp301) that requires a protonated tail causes also a large stabilization of the Cpd I/tyramine cluster and thereby raises the barrier for the Meisenheimer-complex mechanism.

Local Field of the Protein Directs the Preferred Reaction Mechanism. By contrast to the inhibition of the Meisenheimer-complex mechanism, our findings show that CYP2D6 easily activates the phenolic O−H bond of protonated tyramine and leads to a stable intermediate, **IM1**, that proceeds to aromatic ring hydroxylation. Figure 5 (models A vs D) reveals the crucial role of the protein. Thus, as shown in Figure 5 model-A, the gas-phase H-abstraction of the bare protonated tyramine by Cpd I is an endothermic reaction that does not lead to a stable intermediate (see also Figure S5 in Supporting Information). By contrast, as shown in model D, the protein environment stabilizes the intermediate, **IM1**, by as much as 25 kcal mol^{-1} compared with the gas phase and makes the H-abstraction reaction exothermic. Clearly, therefore, the CYP2D6 protein must be the root cause of the stability of the **IM1** intermediate and for generating a corresponding low-energy transition state (Figure 2).

dx.doi.org/10.1021/ja201665x |*J. Am. Chem. Soc.* 2011, 133, 7977–7984

To identify which residues in the active site contribute to this remarkable stabilization of the **IM1**, we performed gas-phase calculations on two QM-only systems, one model included Asp301 (model B in Figure 5) and another model included both Asp301 and Glu216 (model C in Figure 5). Including Asp301 in our QM model stabilizes the **IM1** by 9.6 kcal mol^{-1} compared with model A. Approximately half (4.3 kcal mol^{-1}) of the stabilization can be assigned to a decrease in phenolic O−H bond dissociation energy caused by Asp301. In model C the second nearest polar residue Glu216 was included and stabilized the **IM1** with additionally 6.6 kcal mol^{-1}. Thus, the two charged residues Asp301 and Glu216 close to the reaction center and which bind the tyramine are responsible for stabilizing the **IM1** by 16.2 kcal mol^{-1} of the total 25 kcal mol^{-1} in QM/MM. But what is the cause of the remaining 8−9 kcal mol^{-1} of QM/MM stabilization (in Figure 5D)? Adding other charged residues further away, up to 10 Å, from the reaction center was not helpful, and in fact, they destabilized **IM1** (Table S6 in Supporting Information). Therefore, it was clear that in addition to Asp301 and Glu216, the stability of **IM1** must be influenced by the polarizing field of the neutral residues in the proximity of the reaction center. As such, we performed a calculation wherein the MM charges of all the residues within a radius of 3 Å around the reaction center (thus forming a local protein MM environment) were included in the QM calculation. This calculation led to an **IM1** energy of −16.0 kcal mol^{-1}, which is within 3.3 kcal mol^{-1} from the actual QM energy when all MM point charges are included (see energy value out of parentheses in Model D, Figure 5). The energy difference of 3.3 kcal mol^{-1} can be ascribed to van der Waals and exchange repulsion interactions in the actual cavity.

Electrostatic Effect is Not Due to Simple Bulk Polarity. Using a continuum model (COSMO or PCM using $\varepsilon = 5.62$) to approximate an enzymatic bulk polarity on model B cannot at all reproduce the stabilization of **IM1** (see Table S6 in Supporting Information). Clearly therefore, the protein effect found in the above QM calculation, including embedded MM point charges in the 3 Å vicinity of the substrate, which accounts for the QM/MM results, reflects the directional local electric field of the protein (which is roughly oriented in CYP2D6 along the bisector of the Fe−O axis and the porphine plane).[27b] This is the manner by which the protein controls and directs the desired mechanism, which is otherwise disfavored energetically and exemplifies the importance of electrostatic interaction in enzyme catalysis.[26]

Furthermore, since the intermediate is sensitive to the local oriented polarization field of the protein, it is entirely conceivable that the mechanism can be tinkered with, also by the application of an oriented external electric field (EEF).[27a,c] Indeed, an EEF oriented along the Fe−O bond with a local field strength of 0.0025 au was found sufficient to modulate the reaction barriers of the two steps in Figure 3 (see Table S7 in the Supporting Information for the EEF on each reaction step). Thus, using a positive EEF oriented from Fe to O and with a strength of $F = +0.0025$ au lowered the H-abstraction barrier by 3.4 kcal mol^{-1}, while the rebound barrier was raised to 21.9 kcal mol^{-1} compared with the field-free reaction. Conversely, flipping the EEF direction to $F = -0.0025$ au reduced the H-abstraction barrier by 0.4 kcal mol^{-1}, and the rebound barrier was lowered to 15.0 kcal mol^{-1}, thus enhancing dopamine formation. As such, much like in the above effect of the native protein, here too, a positively oriented EEF stabilizes **IM1** and hence lowers the H-abstraction barrier but raises the rebound barrier. Interestingly, flipping the EEF to the opposite direction has an optimal effect: It keeps the H-abstraction barrier almost unchanged, while at the same time it lowers the rebound barrier.

The discussion above exemplifies the importance of the local electric field of the protein environment and shows its decisive role in determining the nature of the reaction mechanism. Thus, it is the local field of the protein that makes the H-abstraction step exothermic (see Figure 3) by stabilizing the intermediate relative to the reactant, and as such, it preferentially selects a nonclassical aromatic hydroxylation mechanism. Using a small external electric field with an opposite direction offers an opportunity to optimize the rate of dopamine production.

Experimental Evidence for Phenol Activation in Related Aromatic Hydroxylation Reactions. Indeed, oxidation of phenols via hydrogen atom transfer of the hydroxyl group[2,3,55−59,63−67] has been proposed for oxidation of para-substituted phenols to quinones[63,64] and for oxidation of estradiol and estrone.[65] Furthermore, it has also been suggested that the initial step in the formation of the morphine precursor salutaridine is the H-abstraction from the phenolic hydroxyl group.[66]

Some of the more compelling experimental evidence for phenolic H-abstraction mechanism as the one proposed in Scheme 2b are the following:

(i) For quite a few P450 isoforms, including CYP2D6, the presence of a phenolic group was found to be crucial for the hydroxylation of estrone, estradiol,[67] and para-substuted phenols.[64] When the OH group was replaced by a methoxy group, the aromatic hydroxylation reaction either diminished or did not take place, unless it was demethylated.[67] The fact that not all P450s behaved like this (exceptions were CYP1A2 and 2B6) is interesting and further suggests that the protein plays a dominant role in the choice of the phenolic H-abstraction mechanism over the traditional Meisenheimer mechanism.

(ii) When para-substituted phenols were incubated with rat liver P450 in the presence of $^{18}O_2$ the para-substituent X (X = NO_2, CN, CH_2OH, $COCH_3$, COPh, F, Cl, and Br) was eliminated, and in its place one ^{18}O was incorporated in the final quinone.[64]

(iii) The formation of a phenoxyl radical intermediate, as a result of hydrogen atom abstraction from the phenolic group, has been verified in the case of paracetamol[68] hydroxylation by HRP using ESR detection. It was shown that the failure to detect the phenoxy radical during the reaction with P450 was due to the reduction of the radical by the reducing agents, such as NADPH.

Thus, whenever the aromatic molecule has a hydroxyl group and the hydroxylation takes place at para or ortho positions relative to the hydroxyl group, the phenol-activation mechanism is likely to compete favorably with the direct aromatic hydroxylation via the Meisenheimer mechanism. Such likely examples are the biosynthesis of catecholamines,[6] e.g., octopamine to norepinephrine and synephrine to epinephrine. Ideally, the mechanism proposed herein for tyramine, with a rate-determining π-radical rebound, could have been experimentally verified by phenoxy radical detection, but in view of the role of reducing components,[68] this may not succeed. Another probe would be to replace the phenolic hydrogen atom with deuterium, while using $^{18}O_2$. In such a case, we may tentatively expect to find an $^{18}O-D$ group at the hydroxylation site, provided the deuterium is not completely exchanged and washed into the water environment. Finally, substituting the ortho position of tyramine with deute-

rium would lead to NIH shift[2,3] (migration of the deuterium to adjacent ring position) if the mechanism proceeds via the Meisenheimer-complex but not so if it proceeds via the phenolic H-abstraction mechanism.[64]

CONCLUSIONS

The present study reveals that the reaction mechanism by which CYP2D6 transforms tyramine into dopamine involves initially a phenolic H-abstraction by Cpd I followed by a phenoxyl radical ring rebound thereby forming a keto intermediate, **IM1** (Figure 3). Subsequently, the dopamine is formed by a keto−enol rearrangement via a proton relay mechanism assisted by two water molecules (Figure 4).

This mechanism is entirely concocted by the protein. Thus, the preference of the protein for the protonated tyramine raises the barrier for direct aromatic hydroxylation, while the local electric field of the active site facilitates the H-abstraction/phenoxyl rebound mechanism. In the gas phase, the H-abstraction is endothermic, and there is no transition state (TS) or **IM1** minimum, whereas in the protein, a TS with a low barrier is found and an **IM1** intermediate is formed in an exothermic reaction. Successive calculations of the naked **IM1** species in the presence of the MM charges of the protein residues show that the entire stabilization effect is achieved by the local protein environment, within a radius of 3 Å from the substrate and the iron-oxo. Simple bulk polarity (using a continuum model, COSMO) cannot account for this stabilization effect. It is the oriented local electric field of the active site that stabilizes the intermediate and makes the mechanistic choice. It follows that the protein acts as a charge template whose electric field stabilizes the intermediate, thereby enabling the mechanism. Interestingly, using a small external electric field with an opposite direction to the native field offers an opportunity to optimize the rate of dopamine production. These findings are important for understanding the role and the function of enzymes. The role of electrostatic catalysis was discussed in the pioneering studies of Warshel.[26]

The QM/MM computed activation energy for the H-abstraction/phenoxyl rebound mechanism is low, much lower than the barriers for the traditional Meisenheimer-complex mechanism of aromatic hydroxylations.[20−24] It is therefore possible that this is a general reaction mechanism of drugs, neurotransmitters, and hormones, whenever the aromatic molecule has a hydroxyl group near the site of oxidation. Our results together with previously reported proposals[2,3,55−59] support that oxidation of phenols proceeds via an initial H-abstraction from a phenolic hydroxyl.

ASSOCIATED CONTENT

Supporting Information. Complete citations for refs 28, 43, and 46, Cartesian coordinates of all structures described in this work, tables with group spin densities and charges, and figures.This material is available free of charge via the Internet at http://pubs.acs.org.

AUTHOR INFORMATION

Corresponding Author
sason@yfaat.ch.huji.ac.il

ACKNOWLEDGMENT

The research at the HU is supported by the Israeli Science Foundation (ISF grant 09/53). P.S. acknowledges the Wenner-Gren Foundation for a postdoctoral fellowship.

REFERENCES

(1) Guengerich, F. P. In *Cytochrome P450: Structure, Mechanisms, and Biochemistry*, 3rd ed.; Ortiz de Montellano, P. R., Ed.; Kluwer Academic/Plenum Press: New York, 2005; Ch. 10, pp 377−463.
(2) Ortiz de Montellano, P. R.; De Voss, J. J. In *Cytochrome P450: Structure, Mechanisms, and Biochemistry*, 3rd ed.; Ortiz de Montellano, P. R., Ed.; Kluwer Academic/Plenum Press: New York, 2005; Ch. 6, pp 183−230.
(3) Ortiz de Montellano, P. R.; De Voss, J. J. *Nat. Prod. Rep.* **2002**, *19*, 477–494.
(4) Sono, M.; Roach, M. P.; Coulter, E. D.; Dawson, J. H. *Chem. Rev.* **1996**, *96*, 2841–2887.
(5) Zanger, U. M.; Raimundo, S.; Eichelbaum, M. *Naunyn−Schmiedeberg's Arch. Pharmacol.* **2004**, *369*, 23–37.
(6) Hiroi, T.; Imaoka, S.; Funae, Y. *Biochem. Biophys. Res. Commun.* **1998**, *249*, 838–843.
(7) Haining, R. L.; Nichols-Haining, M. *Pharmacol. Ther.* **2007**, *113*, 537–545.
(8) Niwa, T.; Hiroi, T.; Tsuzuki, D.; Yamamoto, S.; Narimatsu, S.; Fukuda, T.; Azuma, J.; Funae, Y. *Mol. Brain Res.* **2004**, *129*, 117–123.
(9) Yu, A.-M.; Idle, L. J.; Byrd, L. G.; Krausz, K. W.; Küpfer, A.; Gonzalez, F. J. *Pharmacogenetics* **2003**, *13*, 173–181.
(10) Patel, S.; Dulluc, J.; Geffard, M. *Histochemistry* **1986**, *85*, 259–263.
(11) Schyman, P.; Usharani, D.; Wang, Y.; Shaik, S. *J. Phys. Chem. B* **2010**, *114*, 7078–7089.
(12) Guengerich, F. P.; Miller, G. P.; Hanna, I. H.; Sato, H.; Martin, M. V. *J. Biol. Chem.* **2002**, *277*, 33711–33719.
(13) Miller, G. P.; Hanna, I. H.; Nishimura, Y.; Guengerich, F. P. *Biochemistry* **2001**, *40*, 14215–14223.
(14) Groves, J. T. *J. Inorg. Biochem.* **2006**, *100*, 434–447.
(15) Schlichting, I.; Berendzen, J.; Chu, K.; Stock, A. M.; Maves, S. A.; Benson, D. E.; Sweet, R. M.; Ringe, D.; Petsko, G. A.; Sligar, S. G. *Science* **2000**, *287*, 1615–1622.
(16) Denisov, I. G.; Makris, T. M.; Sligar, S. G.; Schlichting, I. *Chem. Rev.* **2005**, *105*, 2253–2277.
(17) Shaik, S.; Kumar, D.; de Visser, S. P.; Altun, A.; Thiel, W. *Chem. Rev.* **2005**, *105*, 2279–2328.
(18) Shaik, S.; Cohen, S.; Wang, Y.; Chen, H.; Kumar, D.; Thiel, W. *Chem. Rev.* **2010**, *110*, 949–1017.
(19) Rittle, J.; Green, M. T. *Science* **2010**, *330*, 933–937.
(20) de Visser, S. P.; Shaik, S. *J. Am. Chem. Soc.* **2003**, *125*, 7413–7424.
(21) Bathelt, C. M.; Ridder, L.; Mulholland, A. J.; Harvey, J. N. *J. Am. Chem. Soc.* **2003**, *125*, 15004–15005.
(22) Bathelt, C. M.; Ridder, L.; Mulholland, A. J.; Harvey, J. N. *Org. Biomol. Chem.* **2004**, *2*, 2998–3005.
(23) Rydberg, P.; Ryde, U.; Olsen, L. *J. Phys. Chem. A* **2008**, *112*, 13058–13065.
(24) Bathelt, C. M.; Mulholland, A. J.; Harvey, J. N. *J. Phys. Chem. A* **2008**, *112*, 13149–13156.
(25) Rowland, P.; Blaney, F. E.; Smyth, M. G.; Jones, J. J.; Leydon, V. R.; Oxbrow, A. K.; Lewis, C. J.; Tennant, M. G.; Modi, S.; Eggleston, D. S.; Chenery, R. J.; Bridges, A. M. *J. Biol. Chem.* **2006**, *281*, 7614–7622.
(26) Warshel, A.; Sharma, P. K.; Kato, M.; Xiang, Y; Liu, H.; Olsson, M. H. *Chem. Rev.* **2006**, *106*, 3210–3235.
(27) (a) Lai, W. Z.; Chen, H.; Cho, K. B.; Shaik, S. *J. Phys. Chem. Lett.* **2010**, *1*, 2082–2087. (b) Cho, K. B.; Hirao, H.; Chen, H.; Carvajal, M. A.; Cohen, S.; Derat, E.; Thiel, W.; Shaik, S. *J. Phys. Chem. A* **2008**, *112*, 13128–13138. (c) Shaik, S.; de Visser, S. P.; Kumar, D. *J. Am. Chem. Soc.* **2004**, *126*, 11746–11749.

(28) Frisch, M. J.; et al. *Gaussian 03*, revision D.01; Gaussian, Inc.: Wallingford, CT, 2004.
(29) Ogliaro, F.; Harris, N.; Cohen, S.; Filatov, M.; de Visser, S. P.; Shaik, S. *J. Am. Chem. Soc.* **2000**, *122*, 8977–8989.
(30) de Visser, S. P.; Ogliaro, F.; Sharma, P. K.; Shaik, S. *J. Am. Chem. Soc.* **2002**, *124*, 11809–11826.
(31) de Visser, S. P.; Ogliaro, F.; Sharma, P. K.; Shaik, S. *Angew. Chem., Int. Ed.* **2002**, *41*, 1947–1951.
(32) Ogliaro, F.; de Visser, S. P.; Shaik, S. *J. Inorg. Biochem.* **2002**, *91*, 554–567.
(33) Becke, A. D. *Phys. Rev. A* **1988**, *38*, 3098–3100.
(34) Becke, A. D. *J. Chem. Phys.* **1993**, *98*, 5648–5652.
(35) Lee, C.; Yang, W.; Parr, R. G. *Phys. Rev. B* **1988**, *37*, 785–789.
(36) Schäfer, A.; Huber, C.; Ahlrichs, R. *J. Chem. Phys.* **1994**, *100*, 5829–5835.
(37) Senn, H. M.; Thiel, W. *Top. Curr. Chem.* **2007**, *268*, 173–290.
(38) Ekins, S.; de Groot, M. J.; Jones, J. P. *Drug Metab. Dispos.* **2001**, *29*, 936–944.
(39) Wolff, T.; Distlerath, L. M.; Worthington, M. T.; Groopman, J. D.; Hammons, G. J.; Kadlubar, F. F.; Prough, R. A.; Martin, M. V.; Guengerich, F. P. *Cancer Res.* **1985**, *45*, 2116–2122.
(40) Guex, N.; Peitsch, M. C. *Electrophoresis* **1997**, *18*, 2714−2723.
(41) Li, H.; Robertson, A. D.; Jensen, J. H. *Proteins* **2005**, *61*, 704–721.
(42) Brooks, B. R.; Burccoleri, R. E.; Olafson, B. D.; States, D. J.; Swaminathan, S.; Karplus, M. *J. Comput. Chem.* **1983**, *4*, 187–217.
(43) Mackerell, A. D., Jr.; et al. *J. Phys. Chem. B* **1998**, *102*, 3586–3616.
(44) Smith, W.; Forester, T. R. *J. Mol. Graphics* **1996**, *14*, 136–141.
(45) Hay, P. J.; Wadt, W. R. *J. Chem. Phys.* **1985**, *82*, 299–310.
(46) Sherwood, P.; et al. *J. Mol. Struct. (THEOCHEM)* **2003**, *632*, 1–28.
(47) Ahlrichs, R.; Bär, M.; Häser, M.; Horn, H.; Kölmel, C. *Chem. Phys. Lett.* **1989**, *162*, 165–169.
(48) Bakowies, D.; Thiel, W. *J. Phys. Chem.* **1996**, *100*, 10580–10594.
(49) Sherwood, P.; de Vries, A. H.; Collins, S. J.; Greatbanks, S. P.; Burton, N. A.; Vincent, M. A.; Hillier, I. H. *Faraday Discuss.* **1997**, *106*, 79–92.
(50) de Vries, A. H.; Sherwood, P.; Collins, S. J.; Rigby, A. M.; Rigutto, M.; Kramer, G. J. *J. Phys. Chem. B* **1999**, *103*, 6133–6141.
(51) Billeter, S. R.; Turner, A. J.; Thiel, W. *Phys. Chem. Chem. Phys.* **2000**, *2*, 2177–2186.
(52) Grimme, S.; Antony, J.; Ehrlich, S.; Krieg, H. *J. Chem. Phys.* **2010**, *132*, 154104.
(53) Lonsdale, R.; Harvey, J. N.; Mulholland, A. J. *J. Phys. Chem. Lett.* **2010**, *1*, 3232–3237.
(54) Tian, Z.; Kass, S. R. *J. Am. Chem. Soc.* **2008**, *130*, 10842–10843.
(55) Derat, E.; Shaik, S. *J. Am. Chem. Soc.* **2006**, *128*, 13940–13949.
(56) Simándi, T. M.; May, Z.; Szigyártó, I. Cs.; Simándi, L. I. *Dalton Trans.* **2005**, 365–368.
(57) Shan, X.; Que, L., Jr. *Proc. Natl. Acad. Sci. U.S.A.* **2005**, *102*, 5340–5345.
(58) Nehru, K.; Jang, Y.; Oh, S.; Dallemer, F.; Nam, W.; Kim, J. *Inorg. Chim. Acta* **2008**, *361*, 2557–2561.
(59) Sastri, C. V.; Lee, J.; Oh, K.; Lee, Y. J.; Lee, J.; Jackson, T. A.; Ray, K.; Hirao, H.; Shin, W.; Halfen, J. A.; Kim, J.; Que, L., Jr.; Shaik, S.; Nam, W. *Proc. Natl. Acad. Sci. U.S.A.* **2007**, *104*, 19181–19186.
(60) Wang, Y.; Yang, C.; Wang, H.; Han, K.; Shaik, S. *ChemBioChem* **2007**, *8*, 277–281.
(61) Wang, Y.; Kumar, D.; Yang, C.; Han, K.; Shaik, S. *J. Phys. Chem. B* **2007**, *111*, 7700–7710.
(62) Santos, R.; Hritz, J.; Oostenbrink, C. *J. Chem. Inf. Model.* **2010**, *50*, 146–154.
(63) Ohe, T.; Mashino, T.; Hirobe, M. *Arch. Biochem. Biophys.* **1994**, *310*, 402–409.
(64) Ohe, T.; Mashino, T.; Hirobe, M. *Drug. Metab. Dispos.* **1997**, *25*, 116–122.
(65) Sarabia, S. F.; Zhu, B. T.; Kurosawa, T.; Tohma, M.; Liehr, J. G. *Chem. Res. Toxicol.* **1997**, *10*, 767–771.
(66) Amann, T.; Zenk., M. H. *Tetrahedron Lett.* **1991**, *32*, 3675–3678.
(67) Stresser, D. M.; Kupfer, D. *Biochemistry* **1997**, *36*, 2203–2210.
(68) Bessems, J. G. M.; de Groot, M. J.; Baede, E. J.; te Koppele, J. M.; Vermeulen, N. P. E. *Xenobiotica* **1998**, *28*, 855–875.